

Chemodynamical signatures of bar resonances in the Galactic disk: current data and future prospects

ADAM WHEELER,¹ IRENE ABRIL-CABEZAS,² WILMA H. TRICK,² FRANCESCA FRAGKOU DI,^{3,2} AND MELISSA NESS^{1,4}

¹*Department of Astronomy, Columbia University, Pupin Physics Laboratories, New York, NY 10027, USA*

²*Max-Planck-Institut für Astrophysik, Karl-Schwarzschild-Str. 1, D-85748 Garching b. München, Germany*

³*European Southern Observatory, Karl-Schwarzschild-Str. 2, D-85748 Garching b. München, Germany*

⁴*Center for Computational Astrophysics, Flatiron Institute, 162 Fifth Avenue, New York, NY 10010, USA*

ABSTRACT

The Galactic disk exhibits complex chemical and dynamical substructure thought to be induced by the bar, spiral arms, and satellites. Here, we explore the chemical signatures of bar resonances in action and velocity space and characterize the differences between the signatures of corotation and higher-order resonances using test particle simulations. Thanks to recent surveys, we now have large homogeneous datasets containing metallicities and kinematics of stars outside the solar neighborhood. We compare the simulations to the observational data from *Gaia* EDR3 and LAMOST DR5, and find weak evidence for a slow bar that associates the “hat” moving group with its outer Lindblad resonance and “Hercules” with corotation. While constraints from current data are limited by their spatial footprint, stars closer in azimuth than the Sun to the bar’s minor axis show much stronger chemodynamical signatures of the bar’s outer Lindblad and corotation resonances in test particle simulations. Future datasets with greater azimuthal coverage, including the final *Gaia* data release, will allow reliable chemodynamical identification of bar resonances.

Keywords: Galaxy: abundances – Galaxy: disk – Galaxy: kinematics and dynamics

1. INTRODUCTION

Gaia (Gaia Collaboration et al. 2016), especially data release 2 (DR2; Gaia Collaboration et al. 2018a), which included radial velocities, has revealed the Galactic disk to be dynamically complex (Gaia Collaboration et al. 2018b; Antoja et al. 2018). Many perturbers are at play, and the specific influence of each is not yet clear. The Galaxy’s bar (e.g. Hunt & Bovy 2018; Fragkoudi et al. 2019a), spiral structure (Quillen et al. 2018; Kawata et al. 2018; Hunt et al. 2018; Antoja et al. 2018; Sellwood et al. 2019; Khanna et al. 2019; Khoperskov et al. 2020), and satellite galaxies (Laporte et al. 2019; Khanna et al. 2019) all affect disk kinematics. Furthermore, Hunt et al. (2019) showed that the signatures of each are difficult to disentangle and that many interpretations of the data are possible. Hilmi et al. (2020) showed that perturbers can interact significantly, further complicating matters.

In this work, we focus on the chemical signatures of the bar in action space, and demonstrate that chemical abundances can aid the identification of bar resonances in the disk and constrain the bar pattern speed, Ω_p . Because most abundances do not change over a star’s lifetime, they trace its birth location, providing a non-dynamical “memory”, that can help distinguish the effects of disk perturbations. Past work on chemistry and dynamics has examined the distribution of metallicities and ages near the Sun or throughout the disk to constrain radial migration (e.g. Schönrich & Binney 2009; Hayden et al. 2015; Martinez-Medina et al. 2016; Khoperskov et al. 2019; Frankel et al. 2020). Recently, Chiba & Schönrich (2021) examined the chemical signature of a decelerating bar. We emphasize the importance of the spatial selection function and the limited azimuthal coverage of current datasets.

The existence of the Milky Way’s bar was first inferred from gas velocities (e.g. de Vaucouleurs 1964; Cohen & Few 1976; Liszt & Burton 1980), then with photometry (Blitz & Spergel 1991; Weiland et al. 1994) and star counts (e.g. Nakada et al. 1991; Whitelock & Catchpole 1992; Weinberg 1992). Over time, its pitch angle has been constrained, with the modern consensus be-

ing that the bar is ahead of the Sun by roughly 27° (Dwek et al. 1995; Binney et al. 1997; Stanek et al. 1997; López-Corredoira et al. 2005; Rattenbury et al. 2007; Cao et al. 2013; Wegg & Gerhard 2013). The bar’s pattern speed, however, is still disputed. Identifying the Hercules moving group, a feature of the local velocity distribution, with the Outer Linblad Resonance yields a pattern speed of roughly $55 \text{ km s}^{-1} \text{ kpc}^{-1}$ (Dehnen 1999, 2000, later Chakrabarty 2007; Minchev et al. 2007, 2010; Antoja et al. 2014; Fragkoudi et al. 2019b). On the other hand, studies of the inner Galaxy suggest that the bar is slower, with a pattern speed of $30\text{--}40 \text{ km s}^{-1} \text{ kpc}^{-1}$ (Weiner & Sellwood 1999; Rodríguez-Fernández & Combes 2008; Long et al. 2013; Wegg et al. 2015; Sormani et al. 2015), and that Hercules could be due to the CR resonance (Pérez-Villegas et al. 2017; Monari et al. 2019a,b; Binney 2020). Recent studies suggest a figure around the upper end of this range (Portail et al. 2017; Clarke et al. 2019; Sanders et al. 2019; Monari et al. 2019b; Bovy et al. 2019).

1.1. Dynamical background: axisymmetric actions and resonances

The primary way the bar impacts the disk is through resonant trapping, which affects stellar orbits with frequencies commensurate with the bar, i.e. for which

$$m(\Omega_p - \Omega_\phi) \approx l\Omega_R \quad , \quad (1)$$

where m and l are small integers with $m > 0$, and Ω_ϕ and Ω_R are the frequencies of azimuthal and radial oscillation, respectively. These orbits librate around their parent orbits, which are closed in the frame that rotates with the bar (Contopoulos & Grosbol 1989; Athanasoulas 1992).

Stars trapped at corotation (CR; $l = 0$) exhibit oscillations around a constant azimuth with respect to the bar. Typical galaxy bars have a dominant Fourier $m = 2$ mode (Buta et al. 2006), which means that $m = 2$ resonances, especially the Outer and Inner Lindblad Resonances (OLR and IRL), with $l = \pm 1$ and $m = 2$, affect the disk strongly. Those with $l = \pm 1$, $m = 1$ and $l = \pm 1$, $m = 4$ (referred to as 1:1 and 1:4, respectively) are generally present, but much less dominant, unless the Fourier $m = 4$ mode of the bar is strong (Hunt & Bovy 2018).

While the true potential of the Milky Way is complex, asymmetric, and time-dependent, we can use an axisymmetric approximate potential model to calculate “axisymmetric actions estimates”, J_ϕ, J_R, J_z , for each star, associated with azimuthal, radial, and vertical motion, respectively (e.g. Binney & Tremaine 2008, chapter 3). The frequencies of these oscillations follow from the

Hamiltonian H_{axi} as

$$\Omega_{\text{axi},i} = \frac{\partial H_{\text{axi}}}{\partial J_i}; \quad i \in \{\phi, R, z\} \quad , \quad (2)$$

which are the same as those in Equation 1 only when the true potential is exactly axisymmetric. From here on, we refer to axisymmetric action estimates simply as *actions*. Unlike true actions, which are conserved but not generally known, these change as the star orbits in a non-axisymmetric potential (e.g. Lynden-Bell & Kalnajs 1972; Sellwood & Binney 2002; Binney 2018; Trick et al. 2021). Stars on orbits resonant with the bar and with small J_z oscillate around negatively-sloped lines in the J_R – J_ϕ plane, with J_R decreasing with increasing J_ϕ along them (Sellwood 2010). We refer to these as axisymmetric resonance lines (ARLs).

Because of the conservation of the Jacobi integral, changes to the axisymmetric actions of stars obey

$$\Delta J_R = \frac{l}{m} \Delta J_\phi \quad (3)$$

to first order (Lynden-Bell & Kalnajs 1972; Sellwood & Binney 2002). Consequentially, corotating stars can undergo changes to their angular momentum, J_ϕ , without being radially heated. Most stars are on near-circular orbits, meaning that scattering at the outer 1:1, 1:4, and 1:2 Linblad resonances preferentially increase eccentricity, J_R , inducing a net outward migration and leading to under- and over-densities on either side of the ARL. See Trick et al. (2021) for a pedagogical introduction and numerical investigation of these effects. Evidence of these processes can be seen in velocity- and action-space density. In this work we investigate the signatures of bar resonances in joint action-metallicity space. We also show that this depends strongly on the location of observed stars, i.e. the spatial selection function.

In sections 2 and 3 we describe the observational data and simulations we use, respectively. In section 4, we show how bar resonances give rise to distinct chemical signatures and compare them to observations. In section 5, we discuss the impact of spatial selection functions and consider the capabilities of future surveys. We conclude in section 6.

2. DATA

We use astrometry from *Gaia* EDR3 (Gaia Collaboration et al. 2020), which includes positions, parallaxes, and proper motions for 1.3×10^9 sources, as well as radial velocities (RVs) for 4×10^6 stars (hereafter the *Gaia* RV sample; these are the same as in DR2). We also use the LAMOST (Cui et al. 2012; Zhao et al. 2012; Deng et al. 2012) DR 5 FGAK sample, which provides RVs

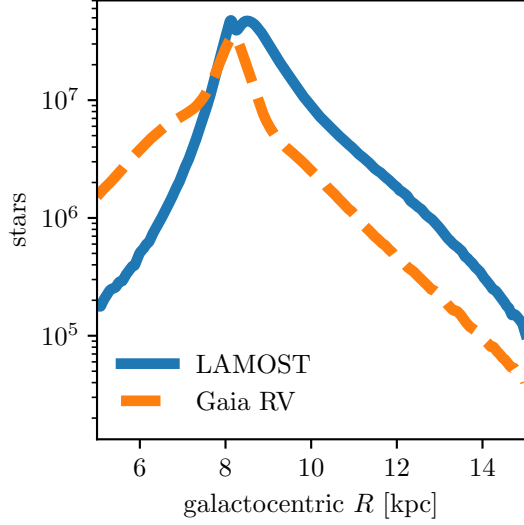


Figure 1. The radial distribution of LAMOST and *Gaia* RV stars. LAMOST RVs can fruitfully augment *Gaia* in the outer disk.

and metallicities for 4.2×10^6 stars from low-resolution ($R \approx 1800$) spectra.

In order to focuss the investigation on near-circular in-plane disk orbits, we used only stars with $J_z < 10 \text{ kpc km s}^{-1}$ and $|z| < 1 \text{ kpc}$. This selection is dominated by thin disk, low- α sequence stars. We also removed the $\sim 1\%$ of stars with L_z outside $1000 - 3000 \text{ kpc km s}^{-1}$ to facilitate comparison with simulations. In order to mitigate magnitude-driven selection effects, we use only LAMOST giants with $2.2 < \log g < 2.7$ and $4500 \text{ K} < T_{\text{eff}} < 5000 \text{ K}$ when dealing with abundances, which often have stellar-parameter-dependent systematics. These cuts leave roughly 800,000 stars when abundances are not needed, and 95,000 when they are.

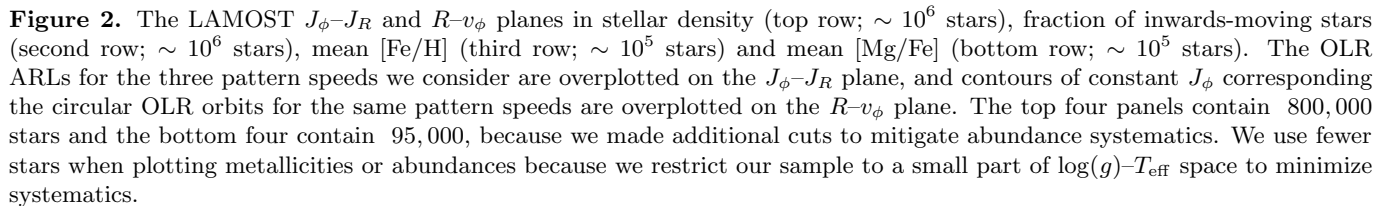
Future *Gaia* data releases will include more RV measurements, but at present, the *Gaia* catalog can be usefully augmented with LAMOST RVs, despite the fact that the latter has a larger typical uncertainty ($\sim 5 \text{ km s}^{-1}$, as opposed to *Gaia*’s $\sim 1 \text{ km s}^{-1}$). Figure 1 shows the radial distribution of LAMOST and *Gaia* RV stars. While there are far more *Gaia* RV than LAMOST stars interior to the Sun, LAMOST has observed more stars at R beyond the Sun. Consequently, *Gaia* and LAMOST together provide a better kinematic picture of the outer disk than *Gaia* alone. What’s more, LAMOST spectra provide metallicities and chemical abundances. We use distance estimates from Bailer-Jones et al. (2018), which used a Galactic prior together with *Gaia* parallax to obtain distance posteriors for stars from both catalogs.

We used *galpy* (Bovy 2015) to calculate actions for each star with the Stäckel fudge (Binney 2012; Bovy & Rix 2013) in the axisymmetric MWPotential2014 model (Bovy 2015). We take the solar Galactocentric radius to be $R_0 = 8 \text{ kpc}$. While kinematic uncertainties propagate to actions, they are small enough not to obscure the chemodynamical signatures we investigate in this paper. Wheeler et al. (2020, Appendix D) show mean action uncertainties as a function of Galactocentric radius, R , for *Gaia* DR2 and LAMOST DR 4, which have RV uncertainties very similar to *Gaia* EDR3 and LAMOST DR 5.

2.1. The MW disk as seen by LAMOST and *Gaia*

Figure 2 shows the *Gaia* + LAMOST R - v_ϕ and J_ϕ - J_R planes in stellar density, fraction of inwards-moving stars, mean $[\text{Fe}/\text{H}]$ and mean $[\text{Mg}/\text{Fe}]$, which is taken from Wheeler et al. (2020), who estimated detailed abundances for LAMOST DR4. Note that $[\text{Fe}/\text{H}]$ and $[\text{Mg}/\text{Fe}]$ increase and decrease, respectively, with increasing J_ϕ , J_R , R , and v_ϕ . While we make use of $[\text{Fe}/\text{H}]$ only in the remainder of this paper, we note that the results presented here can in principle be generalized to other abundances. The ARLs for the OLR of $\Omega_p = 33.5 \text{ km s}^{-1} \text{ kpc}^{-1}$, $39 \text{ km s}^{-1} \text{ kpc}^{-1}$, and $51 \text{ km s}^{-1} \text{ kpc}^{-1}$ are plotted for orientation. In the R - v_ϕ plane, contours of constant angular momentum are overplotted, corresponding to the values of J_ϕ on these OLR ARLs at $J_R = 0$. These pattern speeds, used throughout the paper, correspond to a *fast bar* whose OLR is associated with Hercules ($51 \text{ km s}^{-1} \text{ kpc}^{-1}$), an *intermediate bar* ($39 \text{ km s}^{-1} \text{ kpc}^{-1}$), and a *slow bar* ($33.5 \text{ km s}^{-1} \text{ kpc}^{-1}$). The *intermediate bar* and *slow bar* OLR ARLs align with the “Sirius” and “hat” ridges, respectively, in the $J_\phi - J_R$ plane. The *fast bar* OLR ARL is slightly to the left of the inward-moving ridge that contains the “Horn” stars, and to the right of the outward-moving “Hercules” ridge with which the OLR of a rapidly rotating bar is often associated. The exact values of the *slow bar* and *fast bar* pattern speeds are chosen so that their OLR ARLs align with transitions between net inwards and outwards movement with increasing J_ϕ , as proposed by Trick et al. (2021).

In the R - v_ϕ plane, the ridges identified with *Gaia* (Kawata et al. 2018; *Gaia* Collaboration et al. 2021) and attributed variously to the bar, spiral arms, the Sagittarius dwarf galaxy, or a combination thereof (Antoja et al. 2018; Khanna et al. 2019; Bland-Hawthorn et al. 2019; Fragkoudi et al. 2019a,b; Laporte et al. 2019) are clearly visible. The largest of these can be seen extending to a larger Galactocentric radius, R , than with *Gaia* data alone.



3. SIMULATIONS

To better understand the connection between bar resonance and chemistry in action space, we use test particle simulations with the same pattern speeds introduced in section 2.1 ($\Omega_p = 33.5 \text{ km s}^{-1} \text{ kpc}^{-1}$, $39 \text{ km s}^{-1} \text{ kpc}^{-1}$, and $51 \text{ km s}^{-1} \text{ kpc}^{-1}$). The setup of the simulations is analogous to those used by Trick (2020) and Trick et al. (2021), starting with an axisymmetric disk (Binney & McMillan 2011) of massless particles, followed by integrating stellar orbits in an analytic MW potential model (Bovy 2015) that slowly introduces a bar perturbation (Dehnen 2000; Monari et al. 2016). The boxy bar model has $m = 2$ and $m = 4$ components (Hunt & Bovy 2018) with strengths $\alpha_{m=2} = 0.01$ and weak $\alpha_{m=4} = -0.0005$. Orbits are integrated for 50 bar periods and the simulation snapshots at 20, 30, 40, and 50 bar periods are stacked to increase the number of particles to 4×10^7 .

We assign metallicity values to test particles based on their positions in the initial disk, with a metallicity decreasing with both Galactocentric cylindrical radius R , and height from the midplane, $|z|$. Each particle was assigned an iron abundance according to

$$[\text{Fe}/\text{H}] = -0.09 \left(\frac{R}{\text{kpc}} - 6 \right) + 0.2 - 0.21 \frac{|z|}{\text{kpc}} + \varepsilon, \quad (4)$$

where ε is a random Gaussian perturbation with standard distribution 0.1. The R and z dependence of this relation are based on the trends observed by Hayden et al. (2014) in the low-alpha disk. We note that the qualitative results of this work do not depend on the details of how metallicities are assigned, so long as the dominant trend is decreasing metallicity with Galactocentric radius.

4. RESULTS

4.1. Metallicity signatures of bar resonances in action space

While bar resonances can change J_ϕ and J_R , they can not change a star’s atmospheric metallicity, which remains very-nearly constant over a star’s lifetime. As discussed in Section 1.1, actions oscillate in specific proportions at resonances, so kinematically distinguishing between resonances in observational data is possible in principle. Stellar metallicities, however, provide an orthogonal source of information that makes this task much easier. Figure 3 demonstrates how bar resonances lead to signatures in J_ϕ -[Fe/H] trends at different J_R . The left column shows test particles evolved in an axisymmetric potential and the right shows particles evolved in the barred potential discussed in Section 3. Panels A and B show the R - z plane in metallicity, and

panels C-F show the J_ϕ - J_R plane in both metallicity and density. The bottom two panels show the [Fe/H] trends as a function of J_ϕ , in bins of J_R (panel G shows absolute metallicities, and panel H shows differences with respect to the smallest J_R bin). The error bars in the bottom two panels show the standard error, the scatter in metallicity over the square root of number of stars in each bin. Except at the largest values of J_R and J_ϕ , the standard errors are too small to be visible, indicating that the trends are not due to sampling errors. The colored bands in panels G and H show the range of J_ϕ values each ARL takes on below $160 \text{ kpc km s}^{-1}$. The J_R bin boundaries used in panels G and H are shown as horizontal lines in panels C-F.

Because stars in corotation with the bar oscillate strongly in J_ϕ without changing coherently in J_R (Equation 3), and density changes slowly with J_ϕ , the effect of the corotation resonance is difficult to see in stellar density in the J_ϕ - J_R plane. Contrasting the mean [Fe/H] around the CR ARL for the barred and unbarred simulations reveals that the metallicity gradient becomes shallower when the bar causes stars to librate symmetrically in J_ϕ , washing out the initial metallicity gradient. This flattening is easily visible in panel G, where the metallicity gradient is visibly flattened.

At the other resonances (OLR, 1:1, and 1:4), J_R changes in lockstep with J_ϕ (equation 3). Because of the strong density gradient in J_R (and weaker gradient in J_ϕ), more stars are displaced from near-circular, low- J_R orbits to eccentric, high- J_R orbits than vice versa, creating a density ridge to the right of the corresponding ARL (panel D). Below approximately $J_R = 50 \text{ kpc km s}^{-1}$, the metallicity contours to the right of the OLR ARL are more vertical in the barred simulation because stars on circular orbits have moved upward (and slightly to the right) in the J_ϕ - J_R plane, shifting the mean metallicity up at the location of the overdensity ridge. In panels G and H, the chemical trends around the OLR are most easily identifiable. For near-circular orbits ($0 < J_R [\text{kpc km s}^{-1}] < 15$) in the barred potential, the mean metallicity drops only slightly below that in the unbarred potential. This is because of the small number of lower-metallicity stars scattered from larger J_ϕ and J_R to more circular orbits. In contrast, among the more eccentric stars, the size of the deviation from the overall trend increases with J_R , with trends rising above that of the unbarred potential to form a “wave-crest” in the J_ϕ -[Fe/H] plane across bins of J_R . Like the OLR, the 1:1 and 1:4 resonances create metallicity wave-crests, but they are weaker because of the weaker Fourier $m = 4$ bar component, and the 1:1 comprising stars far beyond the bar.

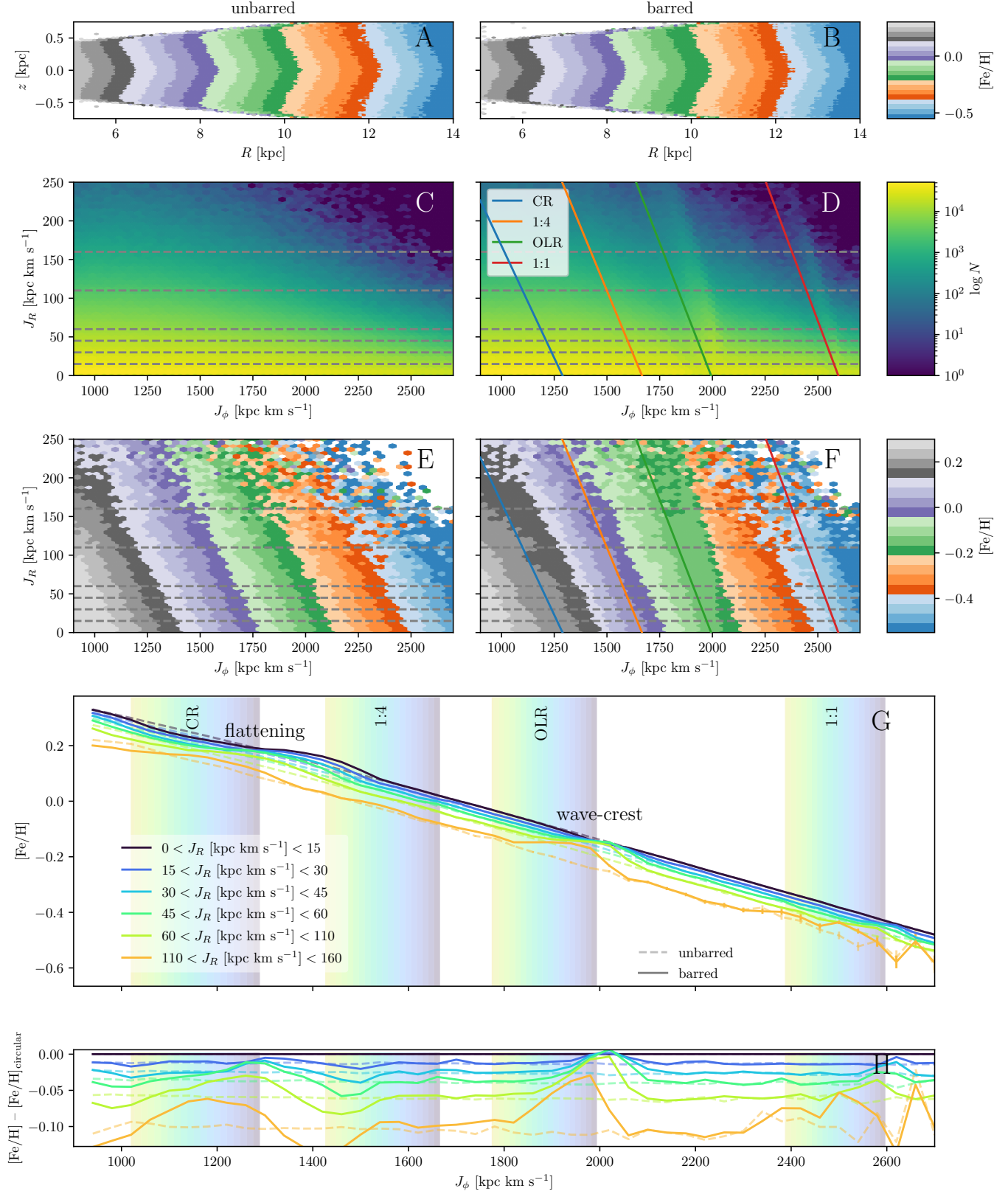


Figure 3. The metallicity signatures at the bar resonances in the *intermediate bar* test particle simulation. **A** and **B**: mean metallicity in the meridional plane for the axisymmetric and barred test particle simulations, respectively. **C** and **D**: number density in the J_ϕ - J_R plane for the axisymmetric and barred test particle simulations, respectively. **E** and **F**: mean $[\text{Fe}/\text{H}]$ in the J_ϕ - J_R plane for the axisymmetric and barred test particle simulations. **G**: mean $[\text{Fe}/\text{H}]$, in bins of J_ϕ and J_R , for the axisymmetric (dashed) and *intermediate bar* (solid) test particle simulations. The CR resonance flattens the mean-metallicity trends, while the higher-order resonances (especially the OLR) create wave-crest signatures. **H**: differences between the above: the difference between mean $[\text{Fe}/\text{H}]$ of each J_R bin and the lowest J_R bin. Error bars in the bottom two panels show the standard error in each bin. Except at the largest values of J_R and J_ϕ , the standard errors are too small to be visible, indicating that the trends are robust. The colored bands show the range of J_ϕ values each ARL takes on below 160 kpc km s $^{-1}$.

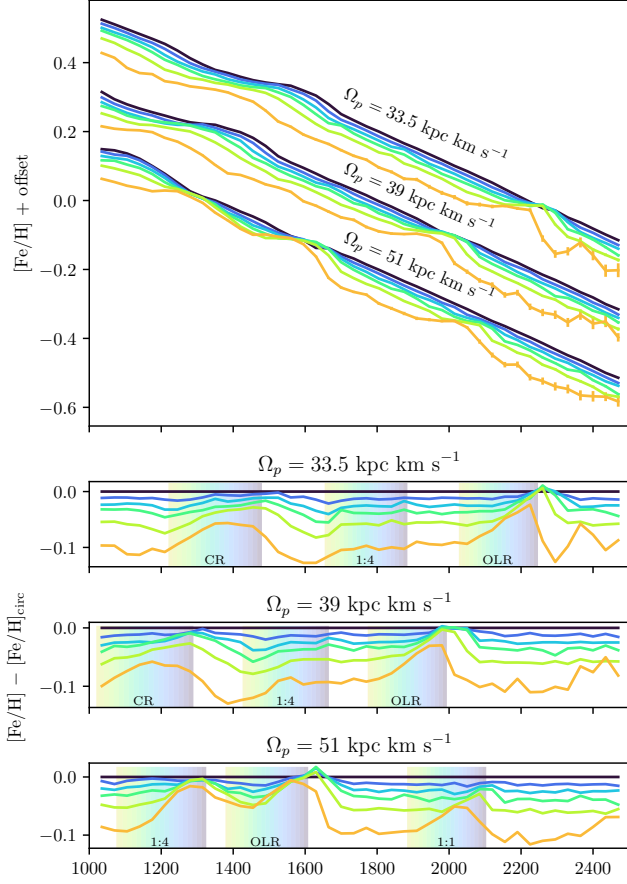


Figure 4. Mean $[\text{Fe}/\text{H}]$ as a function of J_ϕ in bins (same as Figures 3 and 5) of J_R for particles evolved in all three simulations. Error bars show the standard error. The flattening and wave-crest signatures are not sensitive to pattern speed. The vertical bands show the location of ARLs, as in Figure 3.

The wave-crest and flattening signatures at OLR and CR, respectively, in Figure 3 do not change with pattern speed. Figure 4 shows the metallicity trends for particles evolved in all three simulations. While the value of J_ϕ at which the resonances occur changes, the chemical signature of the resonances does not. They do change with bar strength, however. As the bar strength increases, the region of trapped orbits around the ARL becomes larger (c.f. Binney 2018). Figure 5 shows the flattening and wave-crest for the *slow bar* simulation, and for stars evolved in the same potential but with a bar of twice the strength ($\alpha_{m=2} = 0.02$, $\alpha_{m=4} = -0.001$). The flattening in $[\text{Fe}/\text{H}]$ at CR as a function of J_ϕ extends across a larger range of J_ϕ , and the wave-crest at the OLR and 1:1 resonance become more extreme, with the mean metallicity for high- J_R stars exceeding that of those on circular orbits in the resonance zone.

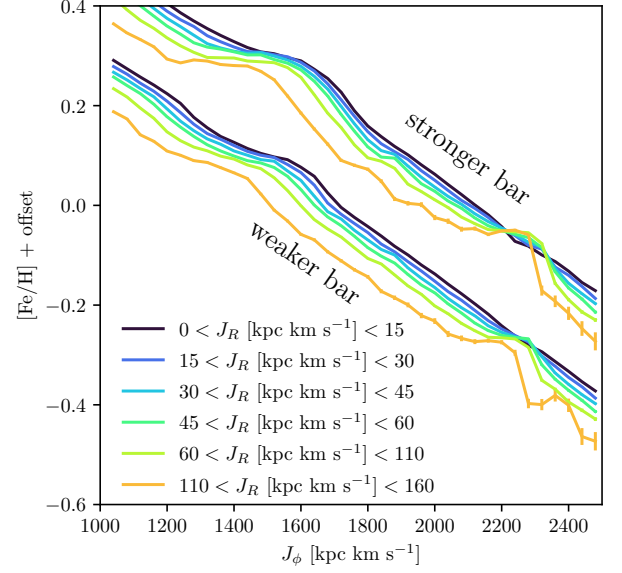


Figure 5. Mean $[\text{Fe}/\text{H}]$ trends in J_ϕ and J_R for two test particle simulations with different bar strengths, but the same pattern speed ($\Omega_p = 33.5 \text{ km s}^{-1} \text{ kpc}^{-1}$). Error bars show the standard error. Because the stronger bar traps more stars on resonant orbits, the metallicity signatures (at $\sim 1500 \text{ kpc km s}^{-1}$ and $\sim 2200 \text{ kpc km s}^{-1}$) cover a larger range in J_ϕ , too.

4.2. Action-metallicity signatures in the LAMOST data

Figure 6 shows mean $[\text{Fe}/\text{H}]$ as a function of J_ϕ and J_R , the diagnostic introduced in section 4.1, drawn with the observational data introduced in Section 2. The three panels show ARL zones corresponding to the three pattern speeds used in the test particle simulations. The limitations of available data (the number of stars observed, their spatial coverage, and uncertainties and biases in their metallicities) make it difficult to clearly identify either the flattening or wave-crest signatures. Only for $\Omega_p = 33.5 \text{ km s}^{-1} \text{ kpc}^{-1}$ are both the CR and the OLR region populated with data, although this is sensitive to the rotation curve of the approximate axisymmetric potential used to calculate actions. Increasing incompleteness with distance from the Sun yields mean- $[\text{Fe}/\text{H}]$ uncertainties large enough to obscure potential resonance signatures for $J_\phi \lesssim 1600 \text{ kpc km s}^{-1}$ and $J_\phi \gtrsim 2700 \text{ kpc km s}^{-1}$, even though some data is present. As we will discuss in section 5.1, the azimuthal coverage of the LAMOST and *Gaia* data also obscure a potential signature of bar resonances.

In the context of the above caveats, we note that the hint of a wave-crest is present in Figure 6 around $J_\phi \approx 2200 \text{ kpc km s}^{-1}$, i.e. close to the Hat moving group. There is a flattening in the mean $[\text{Fe}/\text{H}]$ trend

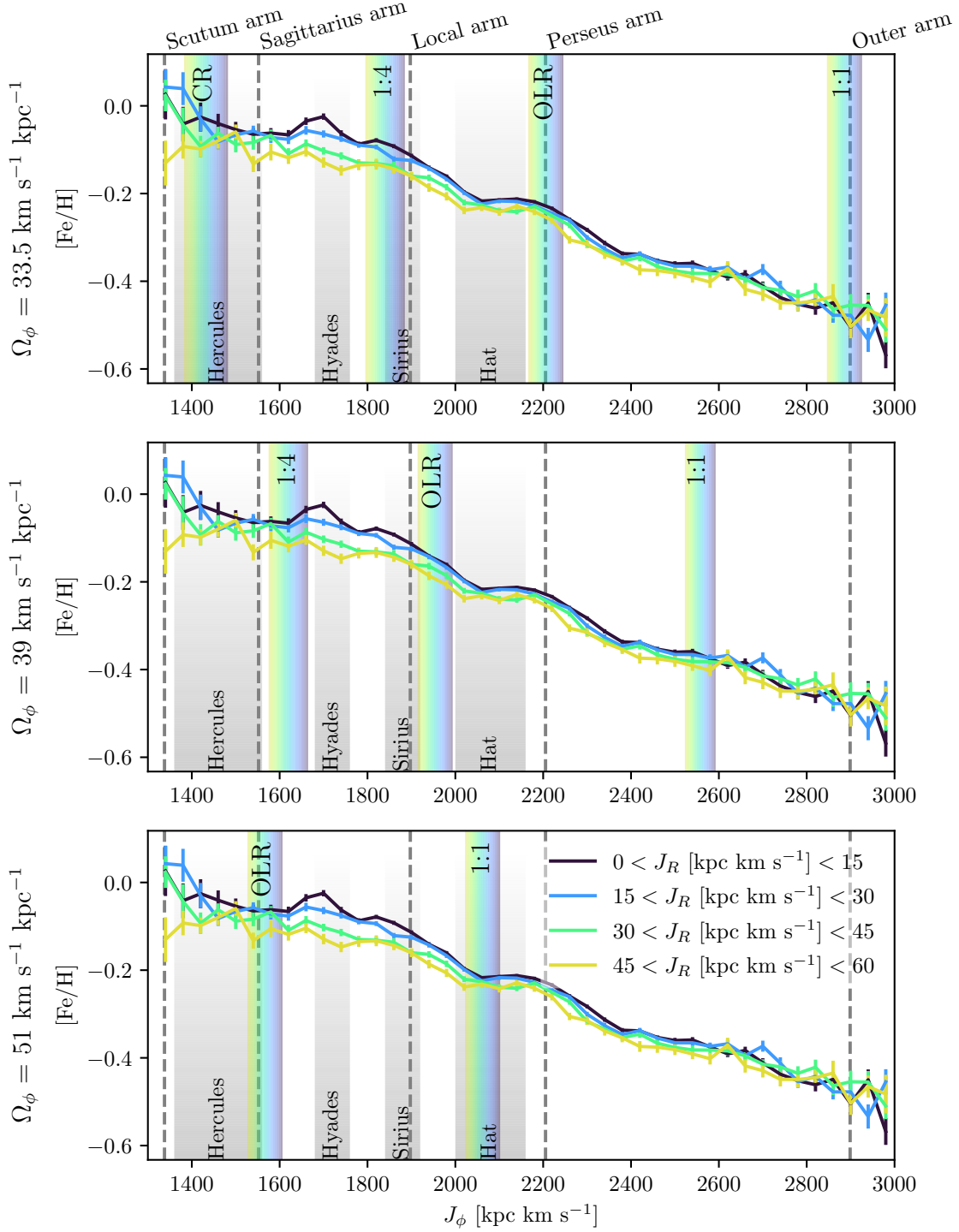


Figure 6. Mean $[\text{Fe}/\text{H}]$ as a function of J_ϕ in bins of J_R for LAMOST. The errorbars show the standard error on the mean. There are not enough stars with $J_R > 60 \text{ kpc km s}^{-1}$ to plot trends. Grey vertical bands mark the approximate J_ϕ of known moving groups for orientation. Gray dashed lines mark the J_ϕ values of circular orbits with R at the radius where the solar azimuth intersects hypothesized spiral arms (taken from Reid et al. 2014). Observational data is not yet plentiful enough to clearly identify or rule out the resonance signatures described in section 4.1, but the flattening around $1400 \text{ kpc km s}^{-1} < J_\phi < 1700 \text{ kpc km s}^{-1}$ and the elbow at $J_\phi \approx 220 \text{ kpc km s}^{-1}$ are suggestive of a slow bar.

at $J_\phi \lesssim 1600$ (which corresponds to $R = 7.5$ kpc). Similar trends have been observed before in the Milky Way (Hayden et al. 2015; Haywood et al. 2018, 2019) and in other galaxies (Stott et al. 2014; Leethochawalit et al. 2016), and have been largely attributed to well-mixed gas, although Hayden et al. (2015) states that stellar migration due to the bar is the likely cause. If the flattening is caused by stellar migration, rather than the birth properties of stars in the inner disk, it is consistent with the CR resonance of a slow (circa 33.5 kpc km s $^{-1}$) bar.

The dependence of mean [Fe/H] on J_R differs strongly across J_ϕ . For $J_\phi \lesssim 2000$ kpc km s $^{-1}$ (at least until $J_\phi \approx 1600$ kpc km s $^{-1}$, when the uncertainties become large), stars on higher-eccentricity orbits have lower [Fe/H]. For $J_\phi \gtrsim 2000$ kpc km s $^{-1}$ the dependence is much weaker. This effect is not a direct consequence of the dependence of [Fe/H] on height from the disk, $|z|$, surface gravity, $\log g$, or effective temperature, T_{eff} . It also does not appear to be caused by “contamination” from the high- α disk, since removing stars with large [Mg/Fe] (per Wheeler et al. 2020) does not have any effect. Additionally, the dependence of mean [Fe/H] on J_R exhibits the same behavior when Figure 6 is made with APOGEE (Majewski et al. 2017) DR16 (Ahumada et al. 2020), rather than LAMOST data. We conclude that it is likely physical, rather than an artifact of the observational data or our analysis.

5. DISCUSSION

5.1. The influence of the spatial selection functions on the metallicity and actions

The bar and spiral arms have been shown to lead to a nonaxisymmetric metallicity distribution (e.g. Di Matteo et al. 2013; Grand et al. 2016; Khoperskov et al. 2018; Fragkoudi et al. 2018), meaning that the spatial location of the observational data with respect to the bar has a significant impact on both the wave-crest and flattening signatures. In contrast to previous Figures, which use stars at all azimuths, Figure 7 shows mean [Fe/H] trends in J_ϕ and J_R using only stars within cylinders centered at different points in the disk for the *intermediate bar* test particle simulation, demonstrating that stars with azimuth nearer to the bar’s minor axis show the resonance signature much more prominently.¹ All cylinders are centered on points 8 kpc from the center of the disk, the approximate Galactocentric radius of the Sun. The first row, which plots stars centered on a

point on the bar’s minor axis (i.e. with $\phi = \phi_\odot - 75^\circ$, taking the bar’s pitch angle to be 25°), exhibits resonance signatures much stronger than the others. For these stars, the flattening at CR turns sharply on and off for each J_R bin, and the OLR wave-crest is very strong, with mean [Fe/H] dependence on J_R fully inverting at $J_\phi \approx 2250$ kpc km s $^{-1}$. For survey volumes centered on the Sun or aligned with the bar’s major axis (rows 2 and 4 in Figure 7), the CR flattening and OLR wave-crest are attenuated and nearly absent, respectively. But if only the stars within 3 kpc of the Sun which are farther from the bar azimuth than the Sun are plotted, both signatures become much more prominent (Figure 7 row 3), demonstrating that a sample in the “extended solar neighborhood” can be used to uncover these features.

Figure 8 shows the degree of CR flattening as a function of position in the disk with two CR orbits plotted, demonstrating again the importance of the azimuth of observed stars and helping to reveal its cause. It is colored by the slope of the J_ϕ -[Fe/H] relation for stars roughly in the *intermediate bar* CR region, with 1200 kpc km s $^{-1} < J_\phi < 1300$ kpc km s $^{-1}$ and $J_R < 60$ kpc km s $^{-1}$, minus the slope outside the CR zone (calculated with the stars in 1600 kpc km s $^{-1} < J_\phi < 1800$ kpc km s $^{-1}$). This figure shows, similarly to Figure 7, that the CR flattening is much stronger in stars around the bar’s minor axis.² The two grey lines show the paths of two stars trapped by the CR resonance as they orbit over 3000 time steps. The azimuthal dependence is a consequence of the “banana” shape of these orbits, which oscillate around Lagrange points 4 and 5 on the bar’s minor axis.

We use a simple rejection sampling scheme to simulate the LAMOST spatial selection function in detail and understand why current data is inadequate to reveal the signatures explored in this work. We approximate the spatial distribution of the test particles and LAMOST stars, $p_{\text{sim}}(\mathbf{r})$ and $p_{\text{LAMOST}}(\mathbf{r})$, where \mathbf{r} is 3D position, by counting the fraction of stars in each bin in a fine grid³, then interpolating with a cubic spline. We then include each test particle in the subset for comparison with probability proportional to the ratio of $p_{\text{sim}}(\mathbf{r})/p_{\text{LAMOST}}(\mathbf{r})$. This reduces the number of particles from 4×10^7 to about 1.6×10^5 , but allows a more “apples to apples” comparison between simulation and

¹ Particles with positive X are rotated 180° to the Sun’s side of the Galaxy to increase the number available to plot.

² There is a weak asymmetry in the metallicity slope at CR around the bar’s minor axis, at about $Y = 4$ kpc, slightly ahead of the minor axis in Figure 8. This is a phase-mixing relic in the simulation which depends on how stars with different initial phases and metallicities get scattered at CR.

³ Bin sizes are 0.5 kpc in the X and Y dimensions, and 0.1 kpc in the z dimension

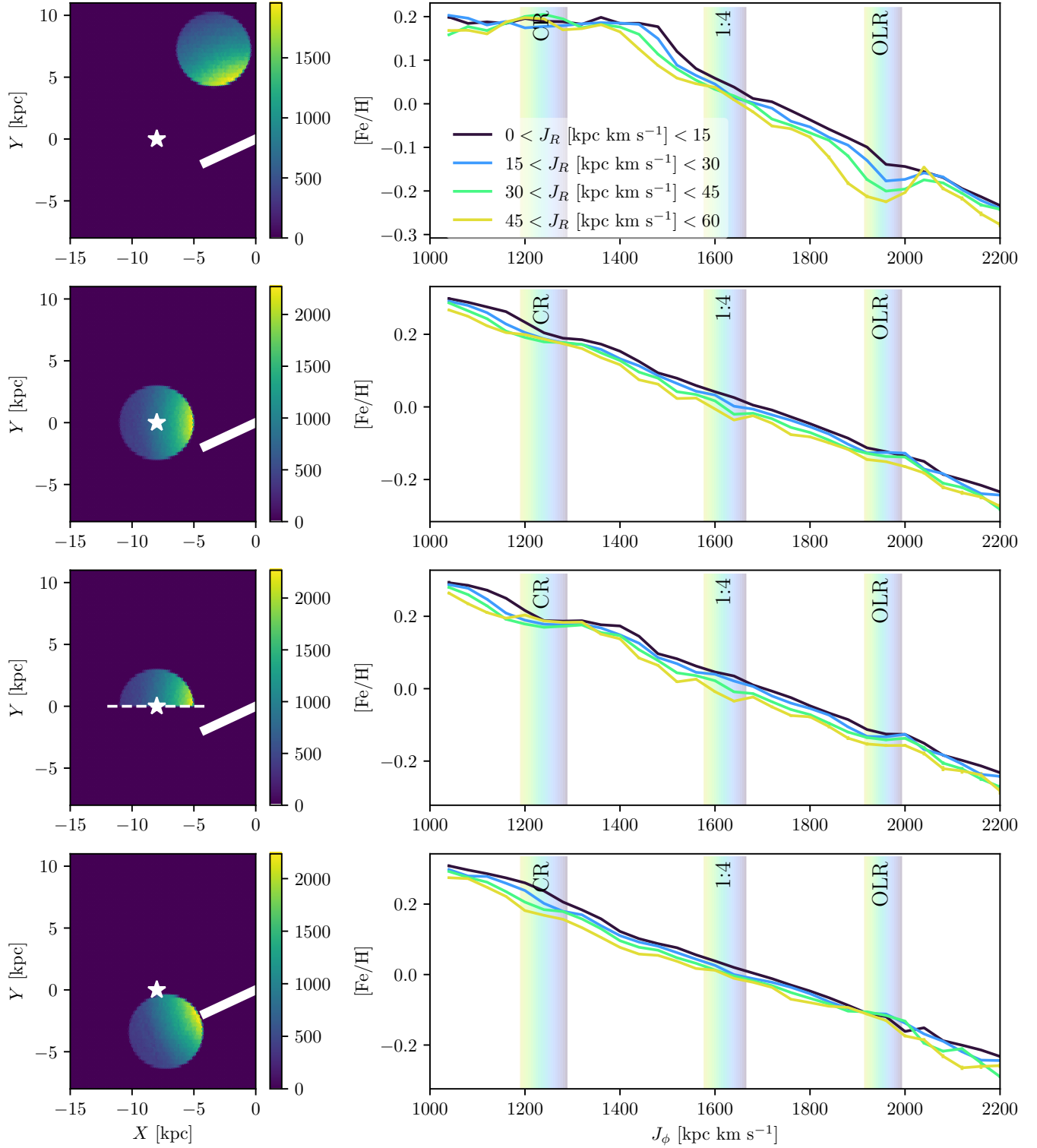


Figure 7. The location of observed stars (i.e. the spatial selection function) has a strong impact on the flattening and wavecrest signatures. Here, resonance signatures as exhibited by stars in different azimuthal regions of the disk in the *intermediate bar* simulation are plotted. J_R bins above 60 kpc km s^{-1} are not plotted because of the lack of sufficient data. Each row shows stars within a cylinder centered at the solar Galactocentric radius at different azimuths: exactly along the minor axis of the bar (top), in the position of the Sun (middle rows), and exactly along the bar's major axis (bottom). The left column shows number density in the X - Y plane, i.e. the footprint of each mock data set in the disk. The white line marks the orientation of the bar, and the white star marks the location of the Sun. The right column shows metallicity trends in J_ϕ and J_R for each region. In row 3, only stars with azimuth farther from the bar azimuth than the Sun are used. The CR flattening and the OLR wavecrest are much more prominent in stars anti-aligned with the bar, but could be seen in a large volume of local data by plotting only stars farther from the bar's azimuth than the Sun (row 3).

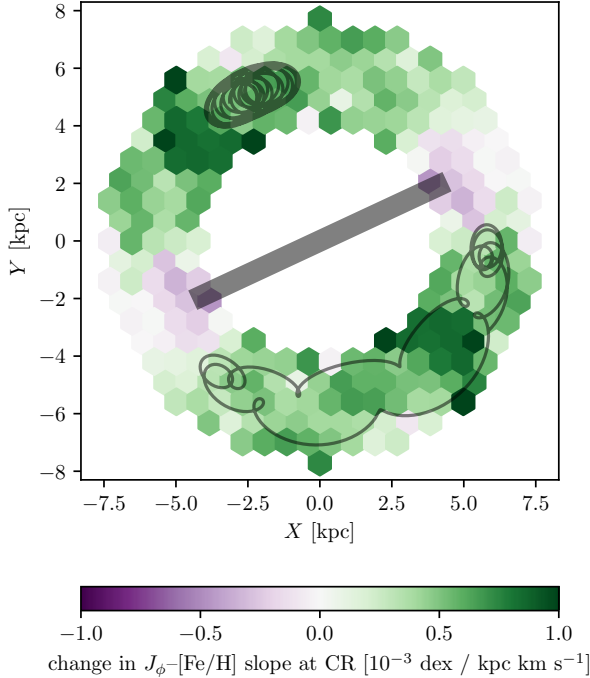


Figure 8. The “banana-shaped” orbits of stars trapped at CR spend little time near the bar’s major axis, and many dwell exclusively near its minor axis, which explains the azimuthal sensitivity demonstrated in Figure 7. The relative slope of the J_ϕ -[Fe/H] relation around CR with respect to the overall slope for stars with $J_R < 60 \text{ kpc km s}^{-1}$ as a function of position in the disk for the *intermediate bar* simulation. The black rectangle indicates the orientation of the bar. The orbits of two stars trapped by the CR resonance are overplotted (in the rotating frame).

data. Figure 9 shows the mean [Fe/H] trends in action space for the *intermediate bar* simulation with the observational spatial footprint imposed. (The results are similar for the *slow bar* and *fast bar* simulations.) Both the wave-crest and flattening are attenuated and distorted by the limited azimuthal coverage. The first row uses the full observational footprint, and the second row uses the same cut as Figure 7 row 3, keeping only stars with azimuth closer to the bar’s minor axis than the Sun. Both selections are too concentrated near the Sun to show the signatures clearly. While LAMOST and other current datasets don’t have the spatial coverage to look for resonance signatures in stars further away from the bar’s major axis, in the near-future metallicities from the *Gaia* RV spectrograph or Sloan-V (Kollmeier et al. 2017) will likely make such an analysis possible.

6. CONCLUSIONS

We investigate the effect of bar resonances on the metallicity distribution in the Milky Way’s thin disk as

a function of the stars’ orbital actions, J_ϕ and J_R . We use test particle simulations of a stellar disk in a Milky-Way-like gravitational potential with a simple rotating bar to identify distinct signatures: The corotation resonance leads to a flattening of the metallicity gradient, and higher-order resonances, especially the Outer Lindblad resonance; this creates a “wave-crest” in the mean [Fe/H] as a function of J_ϕ binned by J_R . We confirm that these signatures do not change qualitatively with pattern speed or strength, although the strength of the signal varies with bar strength. We demonstrate that a survey’s selection function can strongly affect the appearance of these signatures.

We search for these resonant metallicity-vs.-action features in stars using metallicities and RVs from LAMOST DR 5 and parallaxes, proper motions, and supplementary RVs from *Gaia* EDR3. While distinguishing signatures of bar and spiral resonances remains difficult, the diagnostics discussed here can identify both the OLR and CR resonance at once. We find weak evidence for a slow bar associated with the “hat” moving group, but conclude that present data does not allow us yet to unambiguously identify these signatures. Interpreting observational data is made more difficult, not only by the complexities of the Galaxy not present in our simplified test particle model, but also because current surveys provide 6-D kinematics and metallicities only for stars in a limited region of the Galactic disk. In particular, we show that the strength of the flattening and wave-crest signatures depends on the Galactocentric azimuth. The strongest signature is found at an azimuth along the bar’s minor axis, while along the bar’s major axis the resonant signature in the metallicity almost vanishes. Consequently, our observing location within the Galactic disk, $\sim 25^\circ$ behind the bar, is not optimal, but observations of more stars with Galactocentric azimuth far from the major-axis of the bar, which near-future data will deliver, can remedy this.

There are several promising directions for future progress on chemo-dynamically identifying bar resonances. In this paper, we have used a fairly simple galaxy model as basis for the comparison to the data. More complex models may yield modified predictions. For example, a bar with significant deceleration will trap stars with a different distribution of orbits (Chiba et al. 2019), and Chiba & Schönrich (2021) show that metallicity should decrease from the center of the corotation resonance to its boundary. N -body models with self-consistent bars could also provide a richer picture, including the possibly confounding effects spiral arms, which impact metallicity distributions and can overlap with bar resonances. Stellar ages and chemical

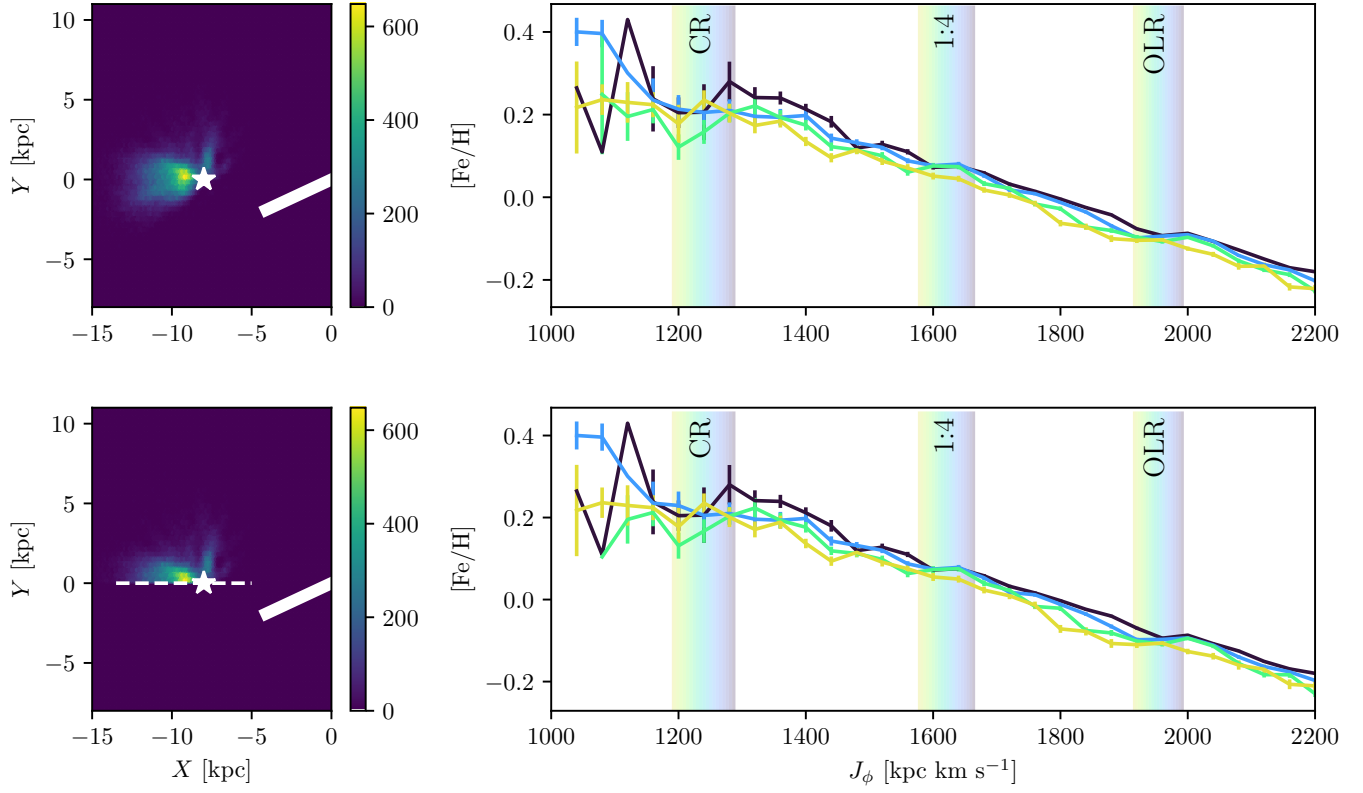


Figure 9. Mean $[\text{Fe}/\text{H}]$ as a function of J_ϕ and J_R for the *intermediate bar* simulation with the LAMOST’s spatial selection function imposed. **top:** full LAMOST footprint. **bottom:** partial LAMOST footprint, with only stars with azimuth less than the Sun’s. The flattening and wave-crest signatures at CR and the OLR, respectively, are extremely attenuated because stars are concentrated near the Sun.

abundances beyond $[\text{Fe}/\text{H}]$ provide additional clues to a star’s birth location and, given a better understanding of the Galaxy’s chemical evolution, can doubtlessly further constrain birth radius. On the other hand, if the bar resonances can be conclusively identified by other means, their chemical abundances inform us on the star formation history of the disk. Sloan V and *Gaia*’s future data releases, which will increase the azimuthal coverage of suitable data, will likely allow us to pinpoint the pattern speed of the bar and shed light on the Galaxy’s dynamical structure.

Software: galpy (Bovy 2015), Matplotlib (Hunter 2007)

ACKNOWLEDGMENTS

The authors would like to thank Jason Hunt, Tomer Yavetz, Kathryn Johnston, and the Milky Way stars group at Columbia for useful discussion and suggestions.

AJW is supported by the National Science Foundation Graduate Research Fellowship under Grant No. 1644869. MKN is in part supported by a Sloan Research Fellowship.

Guoshoujing Telescope (the Large Sky Area Multi-Object Fiber Spectroscopic Telescope LAMOST) is a National Major Scientific Project built by the Chinese Academy of Sciences. Funding for the project has been provided by the National Development and Reform Commission. LAMOST is operated and managed by the National Astronomical Observatories, Chinese Academy of Sciences.

This work has made use of data from the European Space Agency (ESA) mission *Gaia* (<https://www.cosmos.esa.int/gaia>), processed by the *Gaia* Data Processing and Analysis Consortium (DPAC, <https://www.cosmos.esa.int/web/gaia/dpac/consortium>). Funding for the DPAC has been provided by national institutions, in particular the institutions participating in the *Gaia* Multilateral Agreement.

REFERENCES

- Ahumada, R., Allende Prieto, C., Almeida, A., et al. 2020, The Astrophysical Journal Supplement Series, 249, 3, doi: 10.3847/1538-4365/ab929e
- Antoja, T., Helmi, A., Dehnen, W., et al. 2014, Astronomy and Astrophysics, 563, A60, doi: 10.1051/0004-6361/201322623

- Antoja, T., Helmi, A., Romero-Gomez, M., et al. 2018, *Nature*, 561, 360, doi: [10.1038/s41586-018-0510-7](https://doi.org/10.1038/s41586-018-0510-7)
- Athanassoula, E. 1992, *Monthly Notices of the Royal Astronomical Society*, 259, 328, doi: [10.1093/mnras/259.2.328](https://doi.org/10.1093/mnras/259.2.328)
- Bailer-Jones, C. A. L., Rybizki, J., Fouesneau, M., Mantelet, G., & Andrae, R. 2018, *The Astronomical Journal*, 156, 58, doi: [10.3847/1538-3881/aacb21](https://doi.org/10.3847/1538-3881/aacb21)
- Binney, J. 2012, *Monthly Notices of the Royal Astronomical Society*, 426, 1324, doi: [10.1111/j.1365-2966.2012.21757.x](https://doi.org/10.1111/j.1365-2966.2012.21757.x)
- . 2018, *Monthly Notices of the Royal Astronomical Society*, 474, 2706, doi: [10.1093/mnras/stx2835](https://doi.org/10.1093/mnras/stx2835)
- . 2020, *Monthly Notices of the Royal Astronomical Society*, 495, 895, doi: [10.1093/mnras/staa1103](https://doi.org/10.1093/mnras/staa1103)
- Binney, J., Gerhard, O., & Spergel, D. 1997, *Monthly Notices of the Royal Astronomical Society*, 288, 365, doi: [10.1093/mnras/288.2.365](https://doi.org/10.1093/mnras/288.2.365)
- Binney, J., & McMillan, P. 2011, *Monthly Notices of the Royal Astronomical Society*, 413, 1889, doi: [10.1111/j.1365-2966.2011.18268.x](https://doi.org/10.1111/j.1365-2966.2011.18268.x)
- Binney, J., & Tremaine, S. 2008, *Galactic Dynamics: Second Edition*, by James Binney and Scott Tremaine. ISBN 978-0-691-13026-2 (HB). Published by Princeton University Press, Princeton, NJ USA, 2008.
- Bland-Hawthorn, J., Sharma, S., Tepper-Garcia, T., et al. 2019, *Monthly Notices of the Royal Astronomical Society*, 486, 1167, doi: [10.1093/mnras/stz217](https://doi.org/10.1093/mnras/stz217)
- Blitz, L., & Spergel, D. N. 1991, *The Astrophysical Journal*, 379, 631, doi: [10.1086/170535](https://doi.org/10.1086/170535)
- Bovy, J. 2015, *The Astrophysical Journal Supplement Series*, 216, 29, doi: [10.1088/0067-0049/216/2/29](https://doi.org/10.1088/0067-0049/216/2/29)
- Bovy, J., Leung, H. W., Hunt, J. A. S., et al. 2019, arXiv:1905.11404 [astro-ph]. <https://arxiv.org/abs/1905.11404>
- Bovy, J., & Rix, H.-W. 2013, *The Astrophysical Journal*, 779, 115, doi: [10.1088/0004-637X/779/2/115](https://doi.org/10.1088/0004-637X/779/2/115)
- Buta, R., Laurikainen, E., Salo, H., Block, D. L., & Knapen, J. H. 2006, *The Astronomical Journal*, 132, 1859, doi: [10.1086/507696](https://doi.org/10.1086/507696)
- Cao, L., Mao, S., Nataf, D., Rattenbury, N. J., & Gould, A. 2013, *Monthly Notices of the Royal Astronomical Society*, 434, 595, doi: [10.1093/mnras/stt1045](https://doi.org/10.1093/mnras/stt1045)
- Chakrabarty, D. 2007, *Astronomy and Astrophysics*, 467, 145, doi: [10.1051/0004-6361/20066677](https://doi.org/10.1051/0004-6361/20066677)
- Chiba, R., Friske, J. K. S., & Schönrich, R. 2019, arXiv:1912.04304 [astro-ph]. <https://arxiv.org/abs/1912.04304>
- Chiba, R., & Schönrich, R. 2021, arXiv:2102.08388 [astro-ph]. <https://arxiv.org/abs/2102.08388>
- Clarke, J. P., Wegg, C., Gerhard, O., et al. 2019, *Monthly Notices of the Royal Astronomical Society*, 489, 3519, doi: [10.1093/mnras/stz2382](https://doi.org/10.1093/mnras/stz2382)
- Cohen, R. J., & Few, R. W. 1976, *Monthly Notices of the Royal Astronomical Society*, 176, 495, doi: [10.1093/mnras/176.3.495](https://doi.org/10.1093/mnras/176.3.495)
- Contopoulos, G., & Grosbol, P. 1989, *Astronomy and Astrophysics Review*, 1, 261, doi: [10.1007/BF00873080](https://doi.org/10.1007/BF00873080)
- Cui, X.-Q., Zhao, Y.-H., Chu, Y.-Q., et al. 2012, *Research in Astronomy and Astrophysics*, 12, 1197, doi: [10.1088/1674-4527/12/9/003](https://doi.org/10.1088/1674-4527/12/9/003)
- de Vaucouleurs, G. 1964, 20, 195
- Dehnen, W. 1999, *The Astrophysical Journal Letters*, 524, L35, doi: [10.1086/312299](https://doi.org/10.1086/312299)
- . 2000, *The Astronomical Journal*, 119, 800, doi: [10.1086/301226](https://doi.org/10.1086/301226)
- Deng, L.-C., Newberg, H. J., Liu, C., et al. 2012, *Research in Astronomy and Astrophysics*, 12, 735, doi: [10.1088/1674-4527/12/7/003](https://doi.org/10.1088/1674-4527/12/7/003)
- Di Matteo, P., Haywood, M., Combes, F., Semelin, B., & Snaith, O. N. 2013, *Astronomy and Astrophysics*, 553, A102, doi: [10.1051/0004-6361/201220539](https://doi.org/10.1051/0004-6361/201220539)
- Dwek, E., Arendt, R. G., Hauser, M. G., et al. 1995, *The Astrophysical Journal*, 445, 716, doi: [10.1086/175734](https://doi.org/10.1086/175734)
- Fragkoudi, F., Di Matteo, P., Haywood, M., et al. 2018, *Astronomy and Astrophysics*, 616, A180, doi: [10.1051/0004-6361/201732509](https://doi.org/10.1051/0004-6361/201732509)
- Fragkoudi, F., Grand, R. J. J., Pakmor, R., et al. 2019a, arXiv:1911.06826 [astro-ph]. <https://arxiv.org/abs/1911.06826>
- Fragkoudi, F., Katz, D., Trick, W., et al. 2019b, *Monthly Notices of the Royal Astronomical Society*, 488, 3324, doi: [10.1093/mnras/stz1875](https://doi.org/10.1093/mnras/stz1875)
- Frankel, N., Sanders, J., Ting, Y.-S., & Rix, H.-W. 2020, arXiv:2002.04622 [astro-ph]. <https://arxiv.org/abs/2002.04622>
- Gaia Collaboration, Brown, A. G. A., Vallenari, A., et al. 2020, arXiv e-prints, 2012, arXiv:2012.01533
- Gaia Collaboration, Prusti, T., de Bruijne, J. H. J., et al. 2016, *Astronomy and Astrophysics*, 595, A1, doi: [10.1051/0004-6361/201629272](https://doi.org/10.1051/0004-6361/201629272)
- Gaia Collaboration, Brown, A. G. A., Vallenari, A., et al. 2018a, *Astronomy and Astrophysics*, 616, A1, doi: [10.1051/0004-6361/201833051](https://doi.org/10.1051/0004-6361/201833051)
- Gaia Collaboration, Katz, D., Antoja, T., et al. 2018b, *Astronomy & Astrophysics*, 616, A11, doi: [10.1051/0004-6361/201832865](https://doi.org/10.1051/0004-6361/201832865)
- Gaia Collaboration, Antoja, T., McMillan, P., et al. 2021, arXiv e-prints, 2101, arXiv:2101.05811

- Grand, R. J. J., Springel, V., Kawata, D., et al. 2016, *Monthly Notices of the Royal Astronomical Society*, 460, L94, doi: [10.1093/mnrasl/slw086](https://doi.org/10.1093/mnrasl/slw086)
- Hayden, M. R., Holtzman, J. A., Bovy, J., et al. 2014, *The Astronomical Journal*, 147, 116, doi: [10.1088/0004-6256/147/5/116](https://doi.org/10.1088/0004-6256/147/5/116)
- Hayden, M. R., Bovy, J., Holtzman, J. A., et al. 2015, *The Astrophysical Journal*, 808, 132, doi: [10.1088/0004-637X/808/2/132](https://doi.org/10.1088/0004-637X/808/2/132)
- Haywood, M., Di Matteo, P., Lehnert, M., et al. 2018, *Astronomy & Astrophysics*, 618, A78, doi: [10.1051/0004-6361/201731363](https://doi.org/10.1051/0004-6361/201731363)
- Haywood, M., Snaith, O. N., Lehnert, M. D., Di Matteo, P., & Khoperskov, S. 2019, *Astronomy & Astrophysics*, 625, A105, doi: [10.1051/0004-6361/201834155](https://doi.org/10.1051/0004-6361/201834155)
- Hilmi, T., Minchev, I., Buck, T., et al. 2020, *Monthly Notices of the Royal Astronomical Society*, 497, 933, doi: [10.1093/mnras/staa1934](https://doi.org/10.1093/mnras/staa1934)
- Hunt, J. A. S., & Bovy, J. 2018, *Monthly Notices of the Royal Astronomical Society*, 477, 3945, doi: [10.1093/mnras/sty921](https://doi.org/10.1093/mnras/sty921)
- Hunt, J. A. S., Bub, M. W., Bovy, J., et al. 2019, *Monthly Notices of the Royal Astronomical Society*, 490, 1026, doi: [10.1093/mnras/stz2667](https://doi.org/10.1093/mnras/stz2667)
- Hunt, J. A. S., Hong, J., Bovy, J., Kawata, D., & Grand, R. J. J. 2018, *Monthly Notices of the Royal Astronomical Society*, 481, 3794, doi: [10.1093/mnras/sty2532](https://doi.org/10.1093/mnras/sty2532)
- Hunter, J. D. 2007, *Computing in Science Engineering*, 9, 90, doi: [10.1109/MCSE.2007.55](https://doi.org/10.1109/MCSE.2007.55)
- Kawata, D., Baba, J., Ciucă, I., et al. 2018, *Monthly Notices of the Royal Astronomical Society: Letters*, 479, L108, doi: [10.1093/mnrasl/sly107](https://doi.org/10.1093/mnrasl/sly107)
- Khanna, S., Sharma, S., Tepper-Garcia, T., et al. 2019, *Monthly Notices of the Royal Astronomical Society*, 489, 4962, doi: [10.1093/mnras/stz2462](https://doi.org/10.1093/mnras/stz2462)
- Khoperskov, S., Di Matteo, P., Haywood, M., & Combes, F. 2018, *Astronomy and Astrophysics*, 611, L2, doi: [10.1051/0004-6361/201732521](https://doi.org/10.1051/0004-6361/201732521)
- Khoperskov, S., Di Matteo, P., Haywood, M., Gomez, A., & Snaith, O. N. 2019, *arXiv:1911.12424 [astro-ph]*. <https://arxiv.org/abs/1911.12424>
- Khoperskov, S., Gerhard, O., Di Matteo, P., et al. 2020, *Astronomy and Astrophysics*, 634, L8, doi: [10.1051/0004-6361/201936645](https://doi.org/10.1051/0004-6361/201936645)
- Kollmeier, J. A., Zasowski, G., Rix, H.-W., et al. 2017, *arXiv e-prints*, 1711, *arXiv:1711.03234*
- Laporte, C. F. P., Minchev, I., Johnston, K. V., & Gómez, F. A. 2019, *Monthly Notices of the Royal Astronomical Society*, 485, 3134, doi: [10.1093/mnras/stz583](https://doi.org/10.1093/mnras/stz583)
- Leethochawalit, N., Jones, T. A., Ellis, R. S., et al. 2016, *The Astrophysical Journal*, 820, 84, doi: [10.3847/0004-637X/820/2/84](https://doi.org/10.3847/0004-637X/820/2/84)
- Liszt, H. S., & Burton, W. B. 1980, *The Astrophysical Journal*, 236, 779, doi: [10.1086/157803](https://doi.org/10.1086/157803)
- Long, R. J., Mao, S., Shen, J., & Wang, Y. 2013, *Monthly Notices of the Royal Astronomical Society*, 428, 3478, doi: [10.1093/mnras/sts285](https://doi.org/10.1093/mnras/sts285)
- López-Corredoira, M., Cabrera-Lavers, A., & Gerhard, O. E. 2005, *Astronomy and Astrophysics*, 439, 107, doi: [10.1051/0004-6361:20053075](https://doi.org/10.1051/0004-6361:20053075)
- Lynden-Bell, D., & Kalnajs, A. J. 1972, *Monthly Notices of the Royal Astronomical Society*, 157, 1, doi: [10.1093/mnras/157.1.1](https://doi.org/10.1093/mnras/157.1.1)
- Majewski, S. R., Schiavon, R. P., Frinchaboy, P. M., et al. 2017, *The Astronomical Journal*, 154, 94, doi: [10.3847/1538-3881/aa784d](https://doi.org/10.3847/1538-3881/aa784d)
- Martinez-Medina, L. A., Pichardo, B., Moreno, E., & Peimbert, A. 2016, *Monthly Notices of the Royal Astronomical Society*, 463, 459, doi: [10.1093/mnras/stw1997](https://doi.org/10.1093/mnras/stw1997)
- Minchev, I., Boily, C., Siebert, A., & Bienayme, O. 2010, *Monthly Notices of the Royal Astronomical Society*, 407, 2122, doi: [10.1111/j.1365-2966.2010.17060.x](https://doi.org/10.1111/j.1365-2966.2010.17060.x)
- Minchev, I., Nordhaus, J., & Quillen, A. C. 2007, *The Astrophysical Journal Letters*, 664, L31, doi: [10.1086/520578](https://doi.org/10.1086/520578)
- Monari, G., Famaey, B., Siebert, A., et al. 2019a, *Astronomy and Astrophysics*, 632, A107, doi: [10.1051/0004-6361/201936455](https://doi.org/10.1051/0004-6361/201936455)
- . 2016, *Monthly Notices of the Royal Astronomical Society*, 461, 3835, doi: [10.1093/mnras/stw1564](https://doi.org/10.1093/mnras/stw1564)
- Monari, G., Famaey, B., Siebert, A., Wegg, C., & Gerhard, O. 2019b, *Astronomy & Astrophysics*, 626, A41, doi: [10.1051/0004-6361/201834820](https://doi.org/10.1051/0004-6361/201834820)
- Nakada, Y., Onaka, T., Yamamura, I., et al. 1991, *Nature*, 353, 140, doi: [10.1038/353140a0](https://doi.org/10.1038/353140a0)
- Pérez-Villegas, A., Portail, M., Wegg, C., & Gerhard, O. 2017, *The Astrophysical Journal*, 840, L2, doi: [10.3847/2041-8213/aa6c26](https://doi.org/10.3847/2041-8213/aa6c26)
- Portail, M., Gerhard, O., Wegg, C., & Ness, M. 2017, *Monthly Notices of the Royal Astronomical Society*, 465, 1621, doi: [10.1093/mnras/stw2819](https://doi.org/10.1093/mnras/stw2819)
- Quillen, A. C., Carrillo, I., Anders, F., et al. 2018, *Monthly Notices of the Royal Astronomical Society*, 480, 3132, doi: [10.1093/mnras/sty2077](https://doi.org/10.1093/mnras/sty2077)
- Rattenbury, N. J., Mao, S., Debattista, V. P., et al. 2007, *Monthly Notices of the Royal Astronomical Society*, 378, 1165, doi: [10.1111/j.1365-2966.2007.11851.x](https://doi.org/10.1111/j.1365-2966.2007.11851.x)

- Reid, M. J., Menten, K. M., Brunthaler, A., et al. 2014, *The Astrophysical Journal*, 783, 130, doi: [10.1088/0004-637X/783/2/130](https://doi.org/10.1088/0004-637X/783/2/130)
- Rodriguez-Fernandez, N. J., & Combes, F. 2008, *Astronomy and Astrophysics*, 489, 115, doi: [10.1051/0004-6361/200809644](https://doi.org/10.1051/0004-6361/200809644)
- Sanders, J. L., Smith, L., & Evans, N. W. 2019, *Monthly Notices of the Royal Astronomical Society*, 488, 4552, doi: [10.1093/mnras/stz1827](https://doi.org/10.1093/mnras/stz1827)
- Schönrich, R., & Binney, J. 2009, *Monthly Notices of the Royal Astronomical Society*, 396, 203, doi: [10.1111/j.1365-2966.2009.14750.x](https://doi.org/10.1111/j.1365-2966.2009.14750.x)
- Sellwood, J. A. 2010, arXiv:1001.5197 [astro-ph], doi: [10.1111/j.1365-2966.2010.17305.x](https://doi.org/10.1111/j.1365-2966.2010.17305.x)
- Sellwood, J. A., & Binney, J. J. 2002, *Monthly Notices of the Royal Astronomical Society*, 336, 785, doi: [10.1046/j.1365-8711.2002.05806.x](https://doi.org/10.1046/j.1365-8711.2002.05806.x)
- Sellwood, J. A., Trick, W. H., Carlberg, R. G., Coronado, J., & Rix, H.-W. 2019, *Monthly Notices of the Royal Astronomical Society*, 484, 3154, doi: [10.1093/mnras/stz140](https://doi.org/10.1093/mnras/stz140)
- Sormani, M. C., Binney, J., & Magorrian, J. 2015, *Monthly Notices of the Royal Astronomical Society*, 454, 1818, doi: [10.1093/mnras/stv2067](https://doi.org/10.1093/mnras/stv2067)
- Stanek, K. Z., Udalski, A., Szymański, M., et al. 1997, *The Astrophysical Journal*, 477, 163, doi: [10.1086/303702](https://doi.org/10.1086/303702)
- Stott, J. P., Sobral, D., Swinbank, A. M., et al. 2014, *Monthly Notices of the Royal Astronomical Society*, 443, 2695, doi: [10.1093/mnras/stu1343](https://doi.org/10.1093/mnras/stu1343)
- Trick, W. H. 2020, arXiv e-prints, 2011, arXiv:2011.01233
- Trick, W. H., Fragkoudi, F., Hunt, J. A. S., Mackereth, J. T., & White, S. D. M. 2021, *Monthly Notices of the Royal Astronomical Society*, 500, 2645, doi: [10.1093/mnras/staa3317](https://doi.org/10.1093/mnras/staa3317)
- Wegg, C., & Gerhard, O. 2013, *Monthly Notices of the Royal Astronomical Society*, 435, 1874, doi: [10.1093/mnras/stt1376](https://doi.org/10.1093/mnras/stt1376)
- Wegg, C., Gerhard, O., & Portail, M. 2015, *Monthly Notices of the Royal Astronomical Society*, 450, 4050, doi: [10.1093/mnras/stv745](https://doi.org/10.1093/mnras/stv745)
- Weiland, J. L., Arendt, R. G., Berriman, G. B., et al. 1994, *The Astrophysical Journal Letters*, 425, L81, doi: [10.1086/187315](https://doi.org/10.1086/187315)
- Weinberg, M. D. 1992, *The Astrophysical Journal*, 384, 81, doi: [10.1086/170853](https://doi.org/10.1086/170853)
- Weiner, B. J., & Sellwood, J. A. 1999, *The Astrophysical Journal*, 524, 112, doi: [10.1086/307786](https://doi.org/10.1086/307786)
- Wheeler, A., Ness, M., Buder, S., et al. 2020, *The Astrophysical Journal*, 898, 58, doi: [10.3847/1538-4357/ab9a46](https://doi.org/10.3847/1538-4357/ab9a46)
- Whitlock, P., & Catchpole, R. 1992, in *The Center, Bulge, and Disk of the Milky Way*, Vol. 180, 103–110
- Zhao, G., Zhao, Y., Chu, Y., Jing, Y., & Deng, L. 2012, arXiv:1206.3569 [astro-ph], <https://arxiv.org/abs/1206.3569>